High-field electron transport in quantum wires studied by solution of the Boltzmann equation

Toshishige Yamada* and Jun' ichi Sone
Microelectronics Research Laboratories, NEC Corporation, 1-1 Miyazaki, 4-chome, Miyamae-ku, Kawasaki, Kanagawa 213, Japan
(Received 22 January 1988; revised manuscript received 12 May 1989)

High-field electron transport properties in a one-dimensional GaAs quantum wire are studied by a novel method to solve numerically the Boltzmann equation with Fermi-Dirac statistics. The wire is so narrow that quantum subbands are formed. Impurity scattering, optical-phonon scattering, and intersubband scattering are considered in the model. It is shown that two types of electron transport take place, depending on the electron line density and the electric field strength: (1) Electrons are confined to the energy region below the optical-phonon energy Δ under strong optical-phonon scattering around Δ, and (2) they exhibit velocity runaway in the energy region above Δ under decreasing optical-phonon scattering with increasing electron energy.

I. INTRODUCTION

By rapid progress in semiconductor technology it now becomes possible to fabricate one-dimensional semiconductor quantum wires[1-8] with cross-sectional lengths comparable to the electron de Broglie wavelength (~ 10 nm). Since electrons have standing-wave states in the cross-sectional plane in these wires, their motion is restricted in the direction perpendicular to that plane. Thus, their energy levels are quantized and quantum subbands are formed. As a result, their state density becomes different from that for bulk semiconductors, and their transport properties are expected to be greatly changed.

Low-field transport in quantum wires has been studied theoretically by many authors.[9-16] It has been reported that electrons have impurity-limited mobility as large as $10^2 m^2/V\,s$ in degenerate-semiconductor wires at low temperatures where acoustic phonon scattering has little influence on electron transport.[9] It has also been suggested that high-performance quantum-wire devices could be fabricated, taking the advantage of their excellent high mobility.[9]

On the other hand, high-field transport has been discussed rather intuitively[17-20] and two phenomena have been predicted to occur. One is that electrons are confined to the energy region below the optical-phonon energy Δ since they receive strong optical-phonon scattering around Δ due to the one dimensionality.[17,18] The other is that they populate the energy region far above Δ since they receive less optical-phonon scattering with higher energies also due to the one dimensionality.[19,20] The latter case is called velocity runaway.

It is highly interesting to study in what condition confinement or runaway occurs or how the Pauli exclusion principle for electrons affects each phenomenon. In addition, when discussing device applications, the great concern is the transport in high fields where optical-phonon scattering or intersubband (between the different quantum subbands) scattering frequently occurs.

Monte Carlo methods[21] have provided a powerful, effective way to investigate high-field electron transport in bulk semiconductors. However, when applying the ordinary Monte Carlo methods to the quantum wires directly, fluctuations in physical quantities created in each scattering become too large to obtain acceptable values in reasonable computing time. Thus, the Boltzmann equation has to be solved using a powerful computer with a well-refined algorithm, or some other method has to be introduced.

In this paper, a novel method extended from the transport-equation method[22] has been developed to solve numerically the Boltzmann equation and applied to study high-field transport in degenerate-quantum wires. It includes intrasubband and intersubband optical-phonon scattering as well as intrasubband impurity scattering with energy-dependent scattering rates. It solves the Boltzmann equation deterministically without using any random numbers frequently generated in the Monte Carlo method, resulting in no fluctuations in physical quantities. Furthermore, it only assumes that electrons populate according to the Fermi-Dirac distribution functions before the onset of the field, and it does not require any other assumptions used in the previous methods such as for solution forms[23] and for boundary conditions.[24,25]

In Sec. II electron quantum states in quantum wires are shown. In Sec. III the numerical method to solve the Boltzmann equation with the Fermi-Dirac statistics is presented and in Sec. IV the results obtained by this method are discussed. Finally, conclusions are given in Sec. V.

II. ELECTRON STATES IN QUANTUM WIRE

In wires with cross-sectional lengths comparable to the electron de Broglie wavelength (~ 10 nm), electrons have standing-wave states in the cross-sectional plane. Assuming that they populate the parabolic conduction band and are confined in the wire by infinite potential barrier, their wave function ψ and quantized energy E are written by

$$\psi(x,y,z)=A\sin(k_x x)\sin(k_y y)\exp(ik_z z)\ , \tag{1}$$

$$E=\frac{\hbar^2}{2m^*}(k_x^2+k_y^2+k_z^2)\ , \tag{2}$$

$$k_x=N_x\pi L_x^{-1},\quad k_y=N_y\pi L_y^{-1}\ , \tag{3}$$

where x and y indicate the cross-sectional directions and z the line direction. The symbols L_x and L_y are the wire widths in x and y directions, k_z is the continuous wave number in z direction, $\hbar$ the Planck constant, m^* the electron effective mass, and A the normalization constant. Positive integers N_x and N_y are quantum numbers specifying quantum subbands.

The first quantum subband has a state with $N_x=N_y=1$. When $L_x>L_y$, the second quantum subband has a state with $N_x=2$ and $N_y=1$, and the third a state with $N_x=1$ and $N_y=2$. When the wire has the symmetry of $L_x=L_y$, the second subband has twofold degeneracy with $N_x=2$ and $N_y=1$, and with $N_x=1$ and $N_y=2$.

Figures 1(a) and 1(b) show this situation schematically. Figure 1(a) depicts the energy-band structure with three quantum subbands and Fig. 1(b) the state density. The state density is inversely proportional to the square root of energy, diverging at energies where subbands appear. Quantum wires are realized when the energy difference $E_{\rm diff}$ between the first and the second subbands is sufficiently larger than temperature energy so that most of the electrons populate the first subband in an equilibrium state.

Here, high-field electron transport in a 10 nm$\times$10 nm degenerate-GaAs quantum wire at low temperatures is considered. Impurities are assumed to locate in the wire with the line density of 10^7 m^{-1}. In GaAs, the optical-phonon energy Δ is estimated to be 5.60×10^{-21} J and the Γ–L-valley energy difference 5.28×10^{-20} J (9.42Δ). In this wire, the energy difference $E_{\rm diff}$ between the first and the second subbands is 2.68×10^{-20} J (4.78Δ).

Intrasubband scatterings by impurities and intrasubband and intersubband scatterings accompanied by optical-phonon emission are considered in this method. Intersubband scattering by impurities is neglected[26] since the impurity scattering rate decreases rapidly with the electron energy and becomes small enough around $E_{\rm diff}$. The temperatures are assumed to be low enough so that acoustic phonon scattering and optical-phonon absorption scattering can also be neglected. In the fields which will be discussed in the next section, the electron energy is small, so that electrons in the first and the second subbands belonging to the Γ valley are considered.

The scattering rate for each mechanism is written using Fermi's golden rule,

$$\tau^{-1}=\frac{2\pi}{\hbar}|M|^2\rho(E_f)\ , \tag{4}$$

where $\rho(E_f)$ indicates the postscattered state density. The matrix element M is evaluated by using the wave function in Eq. (2) assuming that the electron-phonon

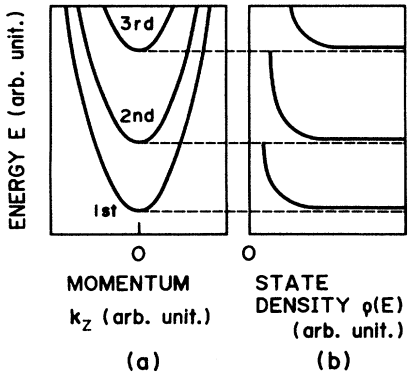

FIG. 1. (a) Electron energy-band structure in a quantum wire with three quantum subbands; (b) electron state density.

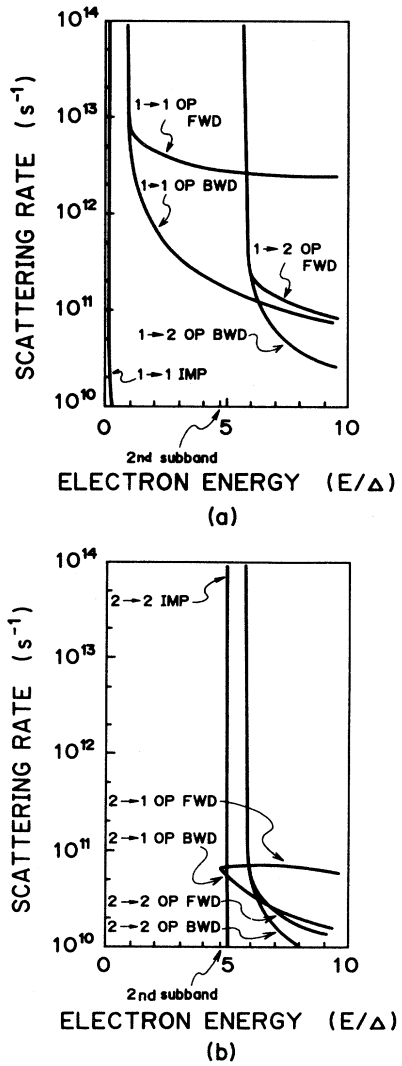

FIG. 2. (a) Scattering rates for electrons in the first subband as a function of electron energy normalized to the optical-phonon energy Δ; (b) scattering rates for electrons in the second subband. Here, $n\rightarrow m$ indicates the transition from the nth to the mth subbands ($n,m=1,2$); IMP, impurity; OP, optical phonon; FWD, forward scattering; and BWD, backward scattering.

coupling constant is the same as that for bulk semiconductors.[27,28] Figure 2(a) shows the calculated scattering rates for electrons in the first subband and Fig. 2(b) for electrons in the second subband. In each figure, intrasubband scatterings in the nth subband are written by $n \rightarrow n$ and intersubband scatterings from the nth to the mth subbands by $n \rightarrow m$ $(n,m=1,2)$. IMP and OP indicate impurity and optical-phonon scatterings, respectively. FWD and BWD stand for forward and backward scatterings, respectively. The electron energy is measured from the bottom of the first subband and normalized to the optical-phonon energy Δ.

As shown in Fig. 2(a), the intrasubband impurity scattering rate diverges at zero energy, the intrasubband optical-phonon scattering rate at Δ, and the intersubband optical-phonon scattering rate at $\Delta+E_{\rm diff}$. Also as shown in Fig. 2(b), the intrasubband impurity scattering rate diverges at $E_{\rm diff}$ and the intrasubband optical-phonon scattering rate at $\Delta+E_{\rm diff}$. The divergences in optical-phonon scattering rates and the decrease in scattering rate for larger energy electrons reflect the energy dependence of the state density in the one-dimensional systems.

In high fields where intrasubband or intersubband optical-phonon scatterings become relevant, the distribution function is expected to become greatly different from the Fermi-Dirac one. This means that the perturbation method starting from the Fermi-Dirac function cannot be applied to the present situation. Thus, the Boltzmann equation has to be solved numerically to study high-field electron transport.

III. NOVEL METHOD TO SOLVE THE BOLTZMANN EQUATION

The wire is assumed to be sufficiently long and the applied electric field spatially uniform so that the distribution function $f(k_z,t)$ does not depend on the space. For simplicity, the variable k_z is changed to the electron total energy E measured from the bottom of the first subband. Then, the distribution function is written by $f_n(E,\pm,t)$, where the signs + and − indicate the direction along and opposite the field, respectively, and the subscript n the nth subband $(n=1,2)$. The Boltzmann equations for f_1 and f_2 can be written by

$$\begin{aligned}
\frac{\partial}{\partial t}f_1(E,\pm,t)+\frac{F}{\hbar}\frac{dE}{dk_z}\frac{\partial}{\partial E}f_1(E,\pm,t)&=T^{11}_{\rm IMP}(E\rightarrow E)\rho_1(E)[f_1(E,\mp,t)-f_1(E,\pm,t)]\\
&+T^{11}_{\rm OPF}(E+\Delta\rightarrow E)\rho_1(E+\Delta)f_1(E+\Delta,\pm,t)[1-f_1(E,\pm,t)]\\
&+T^{11}_{\rm OPB}(E+\Delta\rightarrow E)\rho_1(E+\Delta)f_1(E+\Delta,\mp,t)[1-f_1(E,\pm,t)]\\
&-T^{11}_{\rm OPF}(E\rightarrow E-\Delta)\rho_1(E-\Delta)f_1(E,\pm,t)[1-f_1(E-\Delta,\pm,t)]\theta(E-\Delta)\\
&-T^{11}_{\rm OPB}(E\rightarrow E-\Delta)\rho_1(E-\Delta)f_1(E,\pm,t)[1-f_1(E-\Delta,\mp,t)]\theta(E-\Delta)\\
&+T^{21}_{\rm OPF}(E+\Delta\rightarrow E)\rho_2(E+\Delta)f_2(E+\Delta,\pm,t)[1-f_1(E,\pm,t)]\theta(E+\Delta-E_{\rm diff})\\
&+T^{21}_{\rm OPB}(E+\Delta\rightarrow E)\rho_2(E+\Delta)f_2(E+\Delta,\mp,t)[1-f_1(E,\pm,t)]\theta(E+\Delta-E_{\rm diff})\\
&-T^{12}_{\rm OPF}(E\rightarrow E-\Delta)\rho_2(E-\Delta)f_1(E,\pm,t)[1-f_2(E-\Delta,\pm,t)]\theta(E-\Delta-E_{\rm diff})\\
&-T^{12}_{\rm OPB}(E\rightarrow E-\Delta)\rho_2(E-\Delta)f_1(E,\pm,t)[1-f_2(E-\Delta,\mp,t)]\theta(E-\Delta-E_{\rm diff}),
\end{aligned}\tag{5}$$

$$\begin{aligned}
\frac{\partial}{\partial t}f_2(E,\pm,t)+\frac{F}{\hbar}\frac{dE}{dk_z}\frac{\partial}{\partial E}f_2(E,\pm,t)&=T^{22}_{\rm IMP}(E\rightarrow E)\rho_2(E)[f_2(E,\mp,t)-f_2(E,\pm,t)]\\
&+T^{22}_{\rm OPF}(E+\Delta\rightarrow E)\rho_2(E+\Delta)f_2(E+\Delta,\pm,t)[1-f_2(E,\pm,t)]\\
&+T^{22}_{\rm OPB}(E+\Delta\rightarrow E)\rho_2(E+\Delta)f_2(E+\Delta,\mp,t)[1-f_2(E,\pm,t)]\\
&-T^{22}_{\rm OPF}(E\rightarrow E-\Delta)\rho_2(E-\Delta)f_2(E,\pm,t)[1-f_2(E-\Delta,\pm,t)]\theta(E-\Delta-E_{\rm diff})\\
&-T^{22}_{\rm OPB}(E\rightarrow E-\Delta)\rho_2(E-\Delta)f_2(E,\pm,t)[1-f_2(E-\Delta,\mp,t)]\theta(E-\Delta-E_{\rm diff})\\
&+T^{12}_{\rm OPF}(E+\Delta\rightarrow E)\rho_1(E+\Delta)f_1(E+\Delta,\pm,t)[1-f_2(E,\pm,t)]\\
&+T^{12}_{\rm OPB}(E+\Delta\rightarrow E)\rho_1(E+\Delta)f_1(E+\Delta,\mp,t)[1-f_2(E,\pm,t)]\\
&-T^{21}_{\rm OPF}(E\rightarrow E-\Delta)\rho_1(E-\Delta)f_2(E,\pm,t)[1-f_1(E-\Delta,\pm,t)]\\
&-T^{21}_{\rm OPB}(E\rightarrow E-\Delta)\rho_1(E-\Delta)f_2(E,\pm,t)[1-f_1(E-\Delta,\mp,t)],
\end{aligned}\tag{6}$$

where $T^{nn}_{\mathrm{IMP}}(E\rightarrow E')$ is matrix T (defined by the squared matrix element multiplied by $2\pi/\hbar$) for impurity scattering in the nth subband with prescattered and postscattered energies E and E', $T^{nm}_{\mathrm{OPF}}(E\rightarrow E')$ the matrix T for optical-phonon forward scattering from the nth to the mth subbands, and $T^{nm}_{\mathrm{OPB}}(E\rightarrow E')$ the matrix T for optical-phonon backward scattering from the nth to the mth subbands. The functions $\theta(E)$ indicates the step function; and $\rho_n(E)$ the state density in the nth subband per unit wire length defined by

$$\rho_1(E)=\frac{1}{\pi\hbar}\left[\frac{m^*}{2E}\right]^{1/2}, \tag{7}$$

$$\rho_2(E)=\frac{2}{\pi\hbar}\left[\frac{m^*}{2(E-E_{\mathrm{diff}})}\right]^{1/2}, \tag{8}$$

where the numerical factor 2 due to the electron spin freedom and the factor 2 due to the twofold degeneracy in the second subband by the symmetry in the x-y plane are included.

In this method, energy space is divided into multiple-energy cells with the energy span δE sufficiently smaller than the optical-phonon energy Δ. Electrons populate in accordance with the Fermi-Dirac distribution function up to the onset of the field. Time is also discretized with the period of δt, sufficiently shorter than the inverse of scattering rates. The time evolution of the distribution function is traced every timestep of δt after the onset of the field. Electrons are redistributed among energy cells through scatterings and drift motions according to the following procedure.

First, the electron number N_{scatt} transferred from the kth cell in the nth subband to the lth cell in the mth subband due to scattering mechanism X is written by

$$N_{\mathrm{scatt}}=\delta t\int_{E_{kn}}^{E_{kn}+\delta E}dE\int_{E_{lm}}^{E_{lm}+\delta E}dE'T^{nm}_X(E\rightarrow E')\times\rho_n(E)\rho_m(E')f_n(E)\times[1-f_m(E')]\,, \tag{9}$$

where $T^{nm}_X(E\rightarrow E')$ is matrix T for scattering mechanism X and E_{kn} and E_{lm} the bottom energies for the prescattered and the postscattered cells, and the distribution functions $f_n(E)$ and $f_m(E')$ are for the prescattered and postscattered cells, respectively. Since matrix elements are finite for each scattering mechanism after introducing the electron-screening effect for the impurity, matrix T^{nm}_X varies fairly slowly in a cell. The distribution functions also vary slowly in a cell. Thus, they can be replaced by the values for the central energy in the cells in Eq. (9). Then, the electron transfer number N_{scatt} is expressed by

$$N_{\mathrm{scatt}}=\delta t\,T^{nm}_X(E_{kn}+\delta E/2\rightarrow E_{lm}+\delta E/2)\times f_n(E_{kn}+\delta E/2)[1-f_m(E_{lm}+\delta E/2)]\times\int_{E_{kn}}^{E_{kn}+\delta E}dE\rho_n(E)\int_{E_{lm}}^{E_{lm}+\delta E}dE'\rho_m(E')\,. \tag{10}$$

Two integrals in the above equation correspond to cell-occupation capacities, defined by the maximum electron accommodation numbers in the cells. These capacities do not diverge due to the integration procedure although the integrals contain the singular state densities.

After the electrons are redistributed among cells by scatterings, the electron number distribution in energy cells is transformed into that in momentum space. The momentum for each electron is increased by the amount of $eE\delta t$ due to the drift motion. Then, the electron number distribution is inversely transformed into that in energy space, and the electron number in each energy cell after the time period of δt is determined.

A new distribution function is evaluated by dividing the electron number by the cell-occupation capacity. By repeating these processes, the time evolution of distribution function is studied until a stationary state is reached.

IV. RESULTS AND DISCUSSIONS

In the following, results by the present method are given. It is shown that two types of electron transport corresponding to electron confinement or electron runaway occur, depending on the electron line density and the field strength.

Figures 3(a)–3(e) show the former example for electron transport. The field strength is 1×10^4 V/m and the electron line density 8.68×10^7 m^{-1}. For convenience, the Fermi energy is used to specify the electron line density hereafter. The line density in this case corresponds to the Fermi energy of 0.3Δ. The spatially uniform electric field

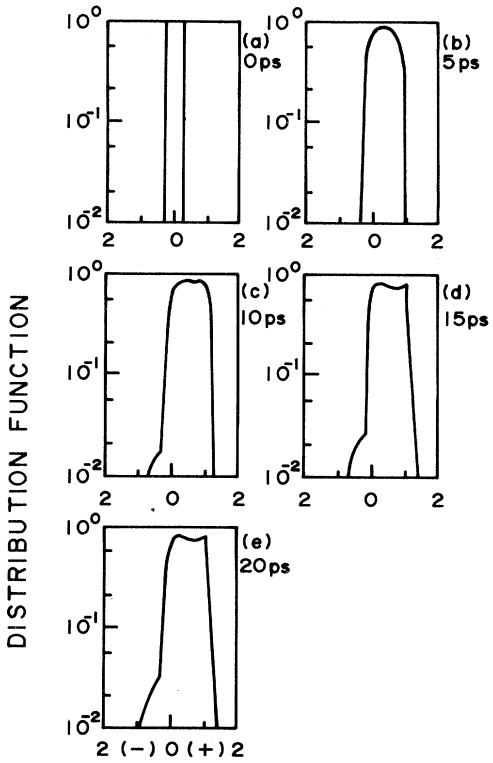

FIG. 3. Time evolution of the distribution function in the field of 1×10^4 V/m with the zero-field Fermi energy of 0.3Δ, showing electron confinement in the region below Δ; the distribution functions (a) at 0 ps, (b) at 5 ps, (c) at 10 ps, (d) at 15 ps, and (e) at 20 ps.

is applied at 0 ps as a step function.

At 0 ps in Fig. 3(a), the distribution function is the Fermi-Dirac one. At 5 ps in Fig. 3(b), it shifts to the positive direction through the drift motion caused by the field. Since electrons receive strong optical-phonon scattering around Δ in the positive direction due to one dimensionality, the function rapidly decreases above Δ in the positive direction.

At 10 ps in Fig. 3(c) and at 15 ps in Fig. 3(d), the function is almost zero except the region between zero energy and the optical-phonon energy. After 10 ps shown in Figs. 3(c)–3(e), the function form is almost the same. The drift velocity and the average energy reach stationary values after around 10 ps. The function after 10 ps is a typical distribution function for electron confinement in the energy region below Δ. It indicates that the electrons are accelerated by the field and when obtaining the energy above Δ, they are scattered by optical phonons into zero energy, repeating these processes.

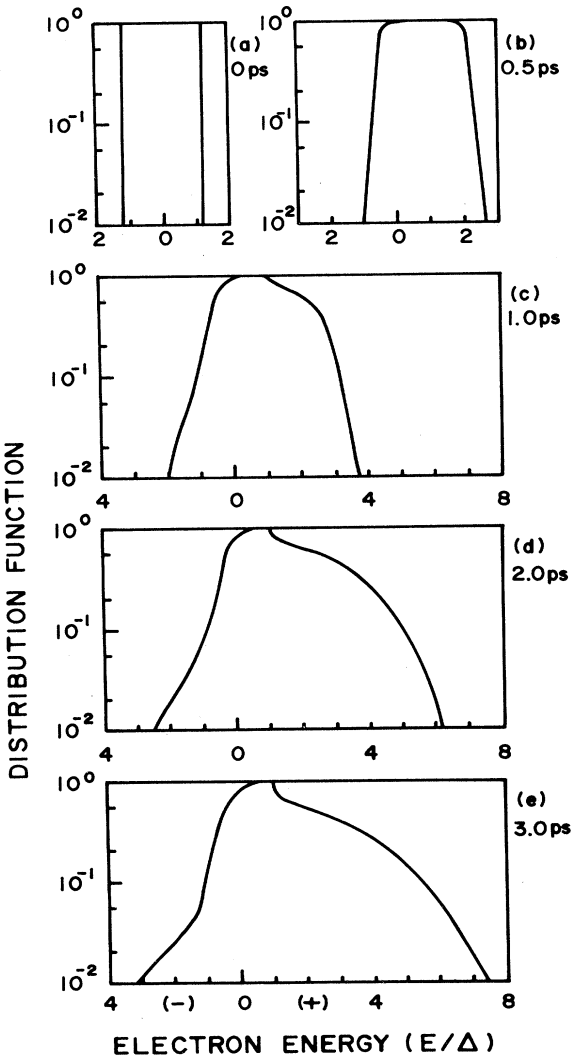

FIG. 4. Time evolution of the distribution function in the field of 1×10^5 V/m with the Fermi energy at 1.2Δ, showing electron velocity runaway above Δ; the distribution functions (a) at 0 ps, (b) at 0.5 ps, (c) at 1.0 ps, (d) at 2.0 ps, and (e) at 3.0 ps.

The period of 10 ps approximately corresponds to the time when electrons obeying the Fermi-Dirac function at the initial stage are accelerated without suffering scatterings finally to have the energy of Δ. After obtaining the energy above Δ, they receive strong optical-phonon scattering and approach their stationary state. The time required for a stationary state to be reached is characterized by the inverse of the optical-phonon scattering rate around Δ. It is estimated to be a few tenths of a picosecond.

Figures 4(a)–4(e) show the latter example for electron transport. The field strength is 1×10^5 V/m and the Fermi energy 1.2Δ, corresponding to the electron line density of 1.74×10^8 m^{-1}. Under this condition, electrons have already occupied the region over Δ in zero field. At 0 ps in Fig. 4(a), the distribution function is the Fermi-Dirac one. At 0.5 ps in Fig. 4(b), it shifts to the right due to the drift motion by the field. Because of the nonlinear dispersion relation between momentum and energy, and optical-phonon backward scattering, the function spreads in both directions. Since the function has the value of almost unity around zero energy, optical-phonon scattering seldom occurs because of the Fermi-Dirac statistics.

At 1.0 ps in Fig. 4(c), the function becomes slightly smaller than unity around zero energy due to the drift motion and the electrons with the energy above Δ begin to receive optical-phonon forward scattering. Thus, the function decreases rapidly above Δ in the positive direction. Because of the nonlinear dispersion relation and the velocity runaway due to the decrease in scattering rate for higher electron energies, the function spreads far in the positive direction. It also spreads in the negative direction because more electrons begin to populate the energy region above Δ in the positive direction and to receive optical-phonon backward scattering.

At 2.0 ps in Fig. 4(d), the function has a notch at Δ, reflecting strong optical-phonon scattering due to the one dimensionality. At 3.0 ps in Fig. 4(e), it spreads farther in both directions, and some electrons receive intersubband scattering and go up to the second subband. The average energy and the electron number in the second subband still gradually increase because of the small intersubband scattering rate of a few tens picoseconds. However, the drift velocity begins to reach the stationary value.

The transport is quite different from that in bulk semiconductors. Because of the sharp onset of optical-phonon emission due to the singular state density, the distribution function has a characteristic structure around Δ. This leads to marked transport patterns of confinement or runaway, depending on what happens to electrons around Δ.

Figure 5 shows the drift velocity as a function of the electric field for various Fermi energies. When the Fermi energy is 0.3Δ, the drift velocity is proportional to the field below the field of 10^4 V/m, with the impurity-limited mobility. In the fields of 10^4 V/m to 10^5 V/m, electron confinement in the energy region below Δ occurs with strong optical-phonon scattering, and the velocity

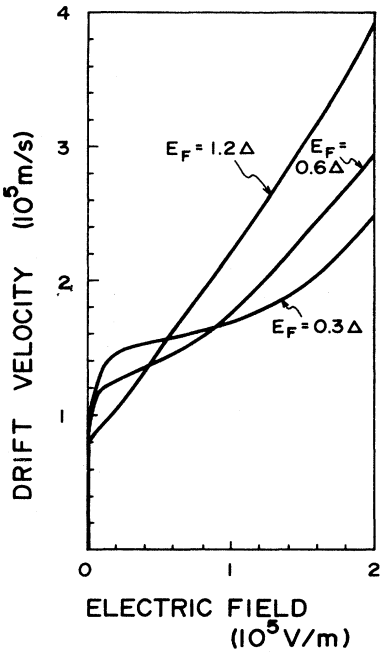

FIG. 5. Electron drift velocity as a function of electric fields for the zero-field Fermi energies of 0.3Δ, 0.6Δ, and 1.2Δ.

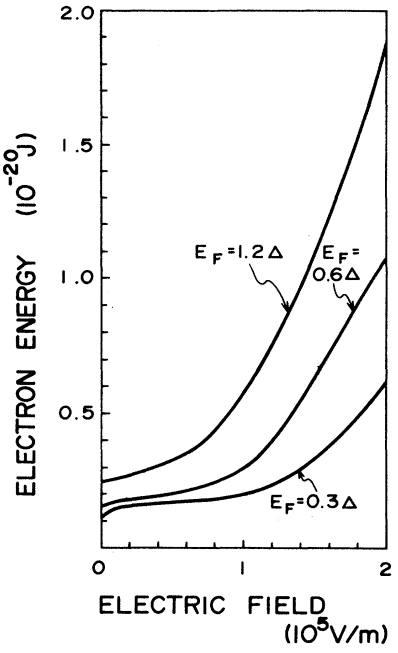

FIG. 7. Average electron energy at 5 ps measured from the bottom of the first subband as a function of electric fields for the zero-field Fermi energies of 0.3Δ, 0.6Δ, and 1.2Δ.

increases slowly with the field. Above the field of 10^5 V/m, the electron runaway occurs, and the velocity rapidly increases with the field. In the field of 2×10^5 V/m, the velocity becomes 2.5×10^5 m/s.

When the Fermi energy is 1.2Δ, some electrons have already had the energy above Δ, and the optical-phonon scattering influences the transport even in lower fields below 10^3 V/m. In the fields higher than 10^3 V/m, electrons with the energy above Δ runaway and the drift velocity rapidly increases with the field. It becomes 3.9×10^5 m/s in the field of 2×10^5 V/m, achieving larger velocity than that of 2.5×10^5 m/s for the Fermi energy of 0.3Δ.

In higher fields where intervalley scattering from Γ to L valleys takes place frequently, the drift velocity will saturate, and negative differential resistance is expected to appear. However, the situation in these fields is out of scope in this work at present.

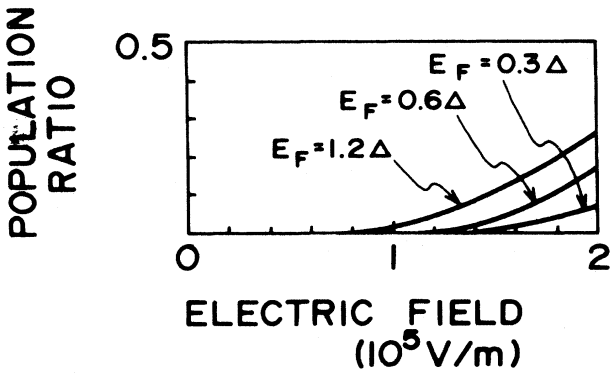

FIG. 6. Population ratio of the second subband electrons to whole electrons at 5 ps as a function of electric fields for the zero-field Fermi energies of 0.3Δ, 0.6Δ, and 1.2Δ.

Figure 6 shows the population ratio of the second subband electrons to the whole electron as a function of the electric field or various Fermi energies. As shown in Fig. 2, the inverse of the scattering rate for the intersubband optical phonon is the order of 10 ps. Thus, the time evolution during a few tens picoseconds has to be traced until a stationary state is reached. Here, the population ratio 5 ps after the onset of the field is plotted. The ratio increases monotonically with the field. Comparing in the same field, the ratio is larger for the larger Fermi energy.

Figure 7 shows the average electron total energy (measured from the bottom of the first subband) 5 ps after the onset of the field as a function of the electric field for various Fermi energies. Comparing in the same field, the average energy is larger for the larger Fermi energy. In zero field, it is equal to one third of the Fermi energy. It increases monotonically with the field. In the field of 2×10^5 V/m, it reaches around 2.0×10^{-20} J (3.6Δ) for the Fermi energy of 1.2Δ, where around 25% of electrons populate the second subband as shown in Fig. 5. In the fields higher than 2×10^5 V/m, the electron number with the energy above 5.28×10^{-20} J (9.42Δ) is not negligible especially for larger Fermi energy. Then, intervalley scatterings from Γ to L valleys have to be considered. It is out of the present formulation.

The results mentioned above are obtained assuming that electrons are confined in a well with an infinite barrier height. However, since the potential barrier is not infinite in a real, physical wire, more subbands appear at low energies. As a result, electrons are transferred to these subbands, and the observation of runaway might become difficult.

Electron-electron scattering is not included in the present model. The effect of this scattering is expected as follows.[29] (1) Since energy exchange among electrons occurs frequently, notches in the distribution function are smeared out. (2) The time for electrons to reach their equilibrium state becomes shorter.

Generalization of the present method taking into account this electron-electron scattering is possible from the simulation-algorithmic point of view. In the electron-electron scattering process at each time step, two arbitrary energy cells are chosen, and electrons are redistributed to the other two energy cells chosen in accordance with energy and momentum conservation law. However, this process requires much more computer memory due to a large number of possible combinations of energy cells.

In this paper, the spatially uniform system has been studied. When considering device applications, it is necessary to study spatially nonuniform systems coupled with the Poisson equation. In order to apply the present method to this problem, the present method needs to be extended to include the spatial dependence of distribution function. These two problems remain for future work.

V. CONCLUSIONS

High-field electron-transport properties in the 10 nm $\times$ 10 nm degenerate-GaAs quantum wire at low temperatures where acoustic phonon scattering has little influence on electron transport have been studied by solving numerically the Boltzmann equation with Fermi-Dirac statistics. Scatterers considered here are intrasubband impurity, intrasubband, and intersubband optical phonons. The following is shown. (1) When the Fermi energy is below Δ, electrons with the energy above Δ receive strong optical-phonon scattering due to the one dimensionality in lower fields. As a result, they are confined to the energy space region below Δ, and the drift velocity rapidly saturates with the increase in field. When the field is further increased over 10^5 V/m, some electrons have the energy above Δ. They receive decreasing optical-phonon scatterings with their increasing energy. Thus, the electron runaway occurs and the drift velocity rapidly increases with the field. (2) When the Fermi energy is above Δ, the electron transport is influenced by optical-phonon scattering even in low fields around 10^3 V/m since some electrons have already had the energy above Δ. Such electrons run away, and the drift velocity rapidly increases with the field. (3) Comparing in higher fields over 10^5 V/m, the drift velocity becomes larger as the Fermi energy increases.

ACKNOWLEDGMENTS

The authors are grateful to H. Abe and Y. Okuto for their continuing encouragement during this work.

*Present address: Center for Solid State Electronics Research, Arizona State University, Tempe, AZ 85287-6206.

[1]W. J. Skocpol, L. D. Jackel, E. L. Hu, R. E. Howard, and L. A. Fetter, Phys. Rev. Lett. **49**, 951 (1982).
[2]W. J. Skocpol, P. M. Mankiewich, R. E. Howard, L. D. Jackel, and D. M. Tennant, Phys. Rev. Lett. **56**, 2865 (1986).
[3]P. M. Petroff, A. C. Gossard, R. A. Logan, and W. Wiegmann, Appl. Phys. Lett. **41**, 196 (1982).
[4]P. M. Petroff, A. C. Gossard, and W. Wiegmann, Appl. Phys. Lett. **45**, 620 (1984).
[5]J. Cibert and P. M. Petroff, Phys. Rev. B **36**, 3243 (1987).
[6]A. B. Fowler, A. Hartstein, and R. A. Webb, Phys. Rev. Lett. **48**, 196 (1982).
[7]A. Hartstein, R. A. Webb, A. B. Fowler, and J. J. Wainer, Surf. Sci. **142**, 1 (1984).
[8]R. G. Wheeler, K. K. Choi, and R. Wisnieff, Surf. Sci. **142**, 19 (1984).
[9]H. Sakaki, Jpn. J. Appl. Phys. **19**, L735 (1980).
[10]J. Lee and H. N. Spector, J. Appl. Phys. **54**, 3921 (1983).
[11]F. A. Riddoch and B. K. Ridley, Surf. Sci. **142**, 260 (1984).
[12]V. A. Arora, J. Phys. C **18**, 3011 (1985).
[13]S. Das Sarma and W. Y. Lai, Phys. Rev. B **32**, 1401 (1985).
[14]P. K. Basu and C. K. Sarkar, Surf. Sci. **174**, 454 (1986).
[15]Perng-fei Yuh and K. L. Wang, Appl. Phys. Lett. **49**, 22 (1986).
[16]Fishman, Phys. Rev. B **34**, 2394 (1986).
[17]W. Shockley, Bell Syst. Tech. J. **30**, 990 (1951).
[18]E. S. Hellman and J. S. Harris, Surf., Sci. **174**, 459 (1986).
[19]H. Fröhlich, Proc. R. Soc. London, Ser. A **172**, 94 (1939).
[20]J. P. Leburton, J. Appl. Phys. **56**, 2850 (1984).
[21]W. Fawcett, A. D. Boadman, and S. Swain, J. Phys. Chem. Solids **31**, 1963 (1970).
[22]L. A. Christel, J. F. Gibbons, and S. Mylroie, J. Appl. Phys. **51**, 6176 (1980).
[23]E. M. Conwell and M. O. Vassel, Phys. Rev. **166**, 797 (1968).
[24]G. D. Mahan, J. Appl. Phys. **58**, 2242 (1985).
[25]G. D. Mahan and G. S. Canright, Phys. Rev. B **35**, 4365 (1987).
[26]K. Yokoyama and K. Hess, Surf. Sci. **174**, 352 (1986).
[27]P. J. Price, Ann. Phys. **133**, 217 (1981).
[28]D. K. Ferry, Surf. Sci. **113**, 199 (1982).
[29]S. M. Goodnick and P. Lugli, Phys. Rev. B **37**, 2578 (1988).